
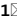




OPEN

Ti-based robust MOFs in the combined photocatalytic degradation of emerging organic contaminants

Sara Rojas^{1,4}, Jessica García-González², Pablo Salcedo-Abraira¹, Irene Rincón¹, Javier Castells-Gil^{3,5}, Natalia M. Padial³, Carlos Marti-Gastaldo³ & Patricia Horcajada¹

Photocatalysis process is a promising technology for environmental remediation. In the continuous search of new heterogeneous photocatalysts, metal–organic frameworks (MOFs) have recently emerged as a new type of photoactive materials for water remediation. Particularly, titanium-based MOFs (Ti-MOFs) are considered one of the most appealing subclass of MOFs due to their promising optoelectronic and photocatalytic properties, high chemical stability, and unique structural features. However, considering the limited information of the reported studies, it is a hard task to determine if real-world water treatment is attainable using Ti-MOF photocatalysts. In this paper, via a screening with several Ti-MOFs, we originally selected and described the potential of a Ti-MOF in the photodegradation of a mixture of relevant Emerging Organic Contaminants (EOCs) in real water. Initially, two challenging drugs (*i.e.*, the β -blocker atenolol (At) and the veterinary antibiotic sulfamethazine (SMT)) and four water stable and photoactive Ti-MOF structures have been rationally selected. From this initial screening, the mesoporous Ti-trimesate MIL-100(Ti) was chosen as the most promising photocatalyst, with higher At or SMT individual photodegradation (100% of At and SMT photodegradation in 2 and 4 h, respectively). Importantly, the safety of the formed by-products from the At and SMT photodegradation was confirmed. Finally, the At and SMT photodegradation capacity of MIL-100(Ti) was confirmed under realistic conditions, by using a mixture of contaminants in tap drinking water (100% of At and SMT photodegradation in 4 h), proven in addition its potential recyclability, which reinforces the potential of MIL-100(Ti) in water remediation.

There is no doubt that pharmaceuticals have efficiently increased life quality and expectancy. However, this exceptional step for humanity has nowadays led to an important environmental issue. Human and veterinary pharmaceuticals, and illicit drugs have been recently defined as Emerging Organic Contaminants (EOCs), being present in biota, sediments, effluents, and surface and ground water¹. Despite their relatively low concentrations in natural waters (few ng·L⁻¹– μ g·L⁻¹), EOCs are of particular concern for several reasons: (1) they have been detected in wastewater treatment plants (WWTPs) and hospitals effluents since these installations are not adapted to eliminate them; (2) many pharmaceuticals have been described recently as endocrine disruptors, raising many questions about risk to the environment and human health²; (3) they can be persistent, and their degradation products can be even more toxic than the parent products³, and (4) drug prescription is expected to sharply increase over the coming decades given the human population growth, the aging population and the drug medical coverage expansion. An increasing number of EOCs in the environment call to not only their monitoring and detection, but also, their efficient elimination.

Among the proposed technologies (*e.g.*, ion-exchange, adsorption and flotation, reverse osmosis)⁴, advanced oxidation processes (AOPs; *e.g.*, photocatalysis, Fenton reactions, sulphate radical mediated oxidations) have attracted a great deal of attention for the water treatment due to their simplicity and reproducibility^{4,5}. In

¹Advanced Porous Materials Unit (APMU), IMDEA Energy Institute. Av. Ramón de La Sagra 3, 28935 Móstoles-Madrid, Spain. ²Department of Nursing, Physiotherapy and Medicine, Faculty of Health Sciences, University of Almería, 04120 Almería, Spain. ³Instituto de Ciencia Molecular, Universitat de València, Catedrático José Beltrán, 2, 46980 Paterna, Spain. ⁴Present address: Department of Inorganic Chemistry, University of Granada, Av. Fuentenueva S/N, 18071 Granada, Spain. ⁵Present address: School of Chemistry, University of Birmingham, Edgbaston, Birmingham B15 2TT, UK. ✉email: srojas@ugr.es; patricia.horcajada@imdea.org

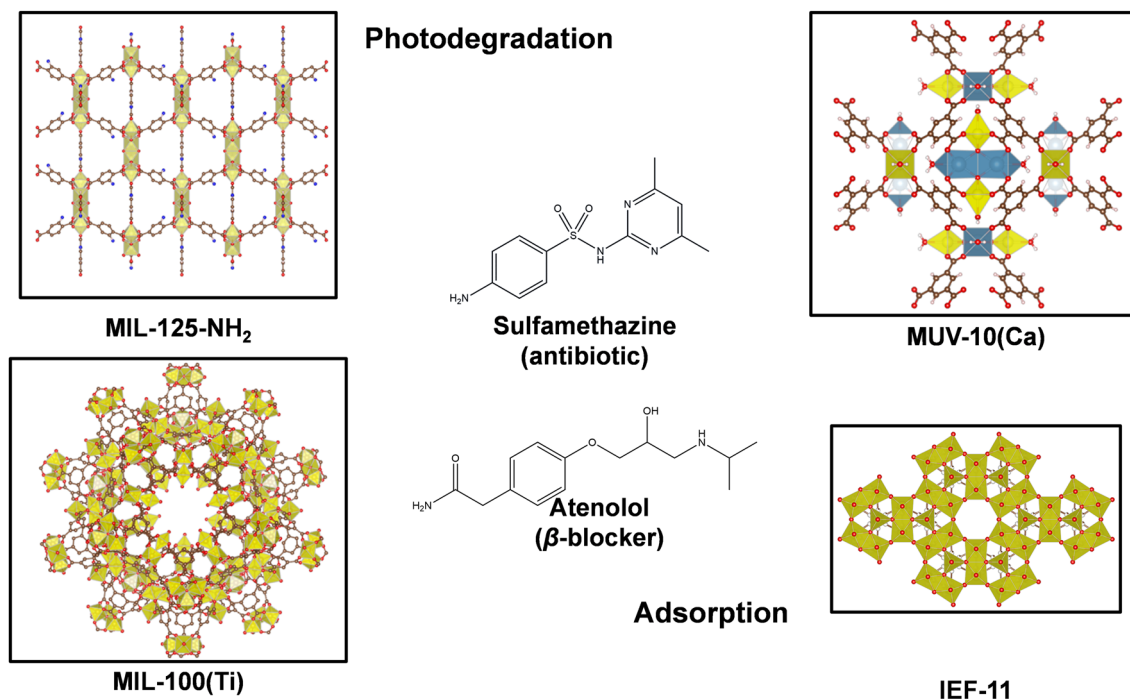


Figure 1. Schematic view of the structure of MIL-125-NH₂, MUV-10(Ca), MIL-100(Ti) and IEF-11 (titanium polyhedra, calcium, oxygen, nitrogen, and carbon are represented in yellow, aegean blue, red, blue, and brown, respectively; hydrogen atoms are omitted for clarity). Structures of the antibiotic SMT and the β-blocker At are also given.

particular, heterogeneous photocatalysts such as TiO₂, ZnO, Fe₂O₃, CdS, GaP, and ZnS have been proposed for the efficient degradation of a wide range of EOCs. However, some of them show typical drawbacks under the operating conditions, like toxicity, low photocurrent quantum yield due to electron hole recombination and/or low solar energy utilization efficiency, resulting from their narrow band gap.

In the continuous search of new semiconductor-based photocatalysts, metal–organic frameworks (MOFs) have recently emerged as a new type of photoactive materials for water remediation. MOFs are an outstanding class of micro/mesoporous coordination polymers, comprising inorganic nodes (*e.g.*, single-atoms, polynuclear clusters, infinite 1D chains) and organic polydentate linkers (*e.g.*, carboxylates, phosphonates, nitrogenated ligands) that assemble into multidimensional periodic lattices⁶. Because of their properties (biocompatibility, porosity, photoactivity, stability, etc.), MOFs have been studied for the degradation of pharmaceuticals. From the first report in the catalytic degradation of an industrial product (phenol) using a MOF in water in 2007⁷, considerable work has been published during the last few years. Particularly, titanium-based MOFs (Ti-MOFs) are considered one of the most appealing subclass of MOFs due to their promising optoelectronic and photocatalytic properties, high chemical stability, and unique structural features^{8,9}. However, compared to other MOFs, the number of Ti-MOF structures is very limited¹⁰. Regarding the EOC removal, only the benchmarked Ti(IV)-aminoterephthalate MIL-125-NH₂ has been reported for this application. In this regard, there are nearly 7 composites based on MIL-125-NH₂ that have shown interesting performances in the EOCs photodegradation. However, prior to the potential use of Ti-MOFs in photoinduced water treatment, some issues need to be tackled, as the majority of the mentioned reports: (1) do not consider the MOF stability (leaching of its components) under working conditions; (2) some of the reported composites are based on highly toxic cations (*i.e.*, MIL-125-NH₂@CdS)¹¹; (3) photocatalytic tests are performed in distilled or Milli-Q water (far from the more complex real water samples); (4) need an equilibrium time (normally 1 h) to reach the EOC adsorption before irradiation or the addition of extra-species to be active (*e.g.*, Na₂SO₄); and/or *v*) study the degradation of just one contaminant, and not a mixture of them, as they are often found in real contaminated water. Although we recently reported a continuous flow system for the photodegradation of sulfamethazine (SMT) using MIL-125-NH₂@Ag nanoclusters¹², the photodegradation of a mixture of contaminants using MOFs and/or their recycling have never been investigated. Therefore, considering the limited information of the reported studies, it is a hard task to determine if real-world water treatment is attainable using Ti-MOFs as photocatalysts.

Accordingly, in the present investigation, we originally described the use of a Ti-MOF in the photodegradation of a mixture of relevant EOCs in real water. Initially, from the large panel of EOCs, and as a result of a thorough research (See Section “**Selection of EOCs**”), two challenging drugs (*i.e.*, the β-blocker atenolol (At) and the veterinary antibiotic sulfamethazine (SMT)) were chosen based on statistic data available in the literature (*i.e.*, exponentially increasing prescription, presence in water, toxic effects, potential development of bacterial resistances, and persistence; see below). Then, for the efficient degradation of these contaminants, we have rationally selected 4 previously reported photoactive highly stable Ti-MOF structures (Fig. 1). In a first step, a fast screening was carried out in tap water to select the most robust MOF with higher At or SMT individual photodegradation,

identifying the mesoporous Ti-trimesate MIL-100(Ti) as the most promising photocatalyst. Subsequently, we have identified the formed by-products from the At and SMT photodegradation, considering their potential toxicity, in order to assess the impact of the MIL-100(Ti) treatment on the resulting water quality. Finally, to deeply evaluate the potential application of MIL-100(Ti) in water remediation, a photodegradation study was carried out under realistic conditions (*i.e.*, mixture of contaminants in tap drinking water, in absence of other co-catalyst/additive, without an adsorption equilibrium time) and considering the potential recyclability, which highlights the originality and interest of this work.

Results and discussion

Selection of EOCs. Among the commonly used 100 pharmaceuticals¹³, anti-hypertensive and antibiotic drugs are two of the most consumed groups. Arterial hypertension is one of the main chronic health problems, being extremely prevalent (20%) among the older adult population¹⁴. β -blockers are among the most consumed drugs used in arterial hypertension treatment¹⁵. During 2020, the consumption of β -blockers ranged around 24,495 (defined daily doses *per* 1,000 inhabitants *per* day)¹⁶. In particular At, a β -blocker drug primarily used to treat patients suffering from various heart disorders such as high blood pressure, chest pain (angina), migraines, and irregular heartbeats¹⁷, was ranked the 31st most prescribed drug in United States of America in 2014¹⁸. In addition, At cannot be fully metabolized by the human body, undergoing incomplete absorption (*ca.* 90%) and being largely excreted unchanged in the urine^{19–21}, exponentially increasing its presence in water (from 0.35 to 2.21 mg·L⁻¹)^{22,23}. Further, the presence of At in water may cause severe toxic effects (*e.g.*, dizziness, feeling tired, depression, chances of heart failure, shortness of breath, and cause bronchospasm), being also accumulated in breast milk, which is related to the immaturity of the renal function of neonate breast-fed infants^{17,24}.

On the other hand, because of their importance for human and veterinary medicine, but also because of their persistence, sulfonamides, quinolones and trimethoprim are the most widely detected antibiotics in water²⁵. Only in Spain, in 2020 the daily dose of prescribed antibiotics by the public health system were 19 *per* 1000 inhabitants *per* day according to the Spanish Agency for Medicines and Health Products. Among the most widely prescribed groups of antibiotics, we can find β -lactams (53.4%), macrolides and lincosamide (11.3%), quinolones (9.8%), tetracycline (8.0%), and sulfonamides and trimethoprim (2.5%)²⁶. Regarding the veterinary use of antibiotics, in the European Union, the bestseller antibiotics were tetracyclines (30.4%), β -lactams (26.9%) and sulfonamides (9.2%)²⁷. Particularly, the sulfonamide sulfamethazine (SMT), frequently used in pigs and cattle, has been detected in natural environments such as soil or water, ranging from a few ng to tens of mg *per* liter or kg of soil^{28,29}. Large proportions of this compound is excreted unchanged in feces and urine given its incomplete metabolism³⁰. Furthermore, the presence of SMT in water is associated with significant risks for humans due to the development of microbial resistances, even at low doses³¹.

Screening of the SMT and At photodegradation and MOF stability. For the efficient removal of EOCs from water, we have selected 4 Ti-MOFs based on: (1) Ti-oxoclusters with redox and photocatalytic activity that could be exploited in the photodegradation of EOCs¹⁰, (2) their *a priori* remarkable hydrolytic stability (mostly tested in pure MilliQ water), (3) their exceptional porosity (see SI, Table S1), in some cases compatible with the SMT and At dimensions ($11 \times 5 \times 5 \text{ \AA}^3$, and $15 \times 7 \times 5 \text{ \AA}^3$, respectively; estimated by Vesta considering van der Waals radii), and (4) in terms of cost, they could be considered affordable for large scale production in the future³². The series comprises: (1) the MIL-100(Ti) or $[\text{Ti}_3(\mu_3\text{-O})\text{O}(\text{OH})_2(\text{BTC})_2]$ (MIL: Materials Institute Lavoisier) based on the trimesate ligand (BTC), which combines a high chemical stability and mesoporosity (~ 25 & 29 \AA , accessible via ~ 5 & 8.6 \AA windows; $S_{\text{BET}} \sim 1300 \text{ m}^2\cdot\text{g}^{-1}$) with photoactive $\text{Ti}_3(\mu_3\text{-O})$ metal-oxoclusters³³; (2) the MIL-125-NH₂ or $[\text{Ti}_8\text{O}_8(\text{OH})_4(\text{BDC-NH}_2)_6]$ built from Ti-oxoclusters coordinated to the 2-aminoterephthalate ligand (BDC-NH₂)³⁴, exhibiting a high microporosity (~ 13 & 6 \AA , accessible via $\sim 6 \text{ \AA}$ windows; $S_{\text{BET}} \sim 1400 \text{ m}^2\cdot\text{g}^{-1}$) and robustness; (3) the MUV-10(Ca) or $[\text{Ti}_3\text{Ca}_3(\mu_3\text{-O})_3(\text{BTC})_4(\text{H}_2\text{O})_6]$ porous solid (MUV: Materials of the University of Valencia) built from the interlinking of fully deprotonated trimesate anions and tetranuclear $\text{Ti}^{\text{IV}}_2\text{Ca}^{\text{II}}_2(\mu_3\text{-O})_2(\text{H}_2\text{O})_4(\text{CO}_2)_8$ clusters³⁵, with an important porosity ($\sim 10 \text{ \AA}$, accessible via $\sim 5 \text{ \AA}$ windows; $S_{\text{BET}} \sim 1000 \text{ m}^2\cdot\text{g}^{-1}$); and (4) the recently reported IEF-11 or $[\text{Ti}_2\text{O}_3(\text{SQ})]$ (IEF: IMDEA Energy Framework)³⁶, based on photo/redox 2D titanium layers and the squarate (SQ, 3,4-dihydroxycyclobut-3-ene-1,2-dionate) as organic linker (see detailed properties in Table S1), with small porosity ($\sim 4.5 \text{ \AA}$; $S_{\text{BET}} \sim 120 \text{ m}^2\cdot\text{g}^{-1}$) but an exceptional hydrolytic stability.

First, the SMT and At photodegradation capacity and the matrix chemical stability of the selected Ti-based MOFs were studied by using similar At and SMT concentrations normally reported in the environment (5 ppm³⁷, and 35 ppm^{38,39}, respectively). The At and SMT photodegradation capacity strongly depends on the used MOF, decreasing in the following order: (At) MIL-100(Ti) > MIL-125-NH₂ > IEF-11 > MUV-10(Ca); and (SMT) MIL-100(Ti) > MIL-125-NH₂ > MUV-10(Ca) > IEF-11 (Fig. 2).

Interestingly, these results highlight the remarkable ability of the MIL-100(Ti) to remove both EOCs, eliminating 100% of At and SMT in only 2 and 4 h, respectively. The plateau of degradation is reached only after 1 h in all studied materials, except for the continuous At degradation of IEF-11, and SMT and At degradation of MIL-100(Ti) where it took only 2 h. Factors like MOF structure/porosity (pore accessibility, surface, volume, tortuosity, connectivity, particle size, etc.) and nature (ligand, cluster structure, band gap, external surface, etc.) might influence the pharmaceuticals degradation capacity. For instance, compared with the rest of studied Ti-MOFs, the lower accessibility of IEF-11, with a pore and window size of 4.5 \AA , might hamper the accessibility of At and SMT and, therefore, their photodegradation. In fact, there is no SMT degradation when using IEF-11 and the kinetics of degradation of At is *ca.* 11-fold lower than MIL-100(Ti) (Table 1). Regarding the chemical nature of MOFs, there is not a direct relationship between the calculated *band gap* values (Fig. S1) and the photocatalytic capacity of these materials in the studied reaction.

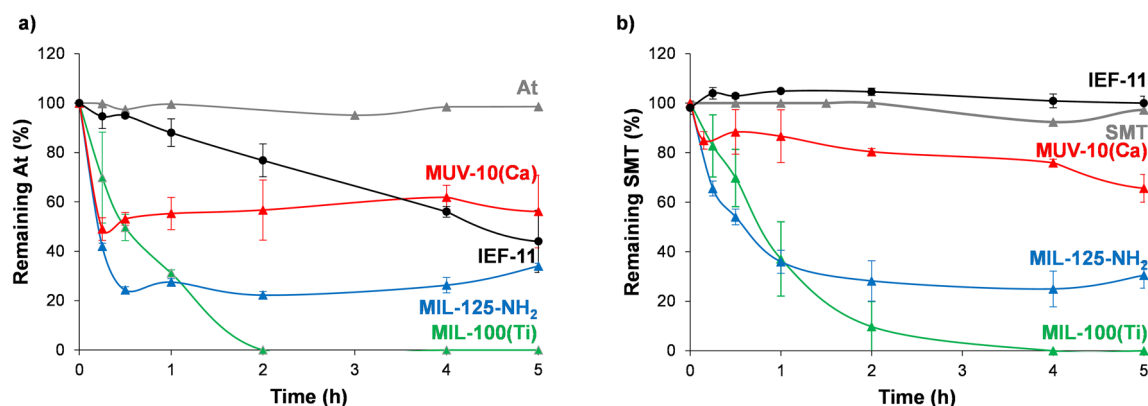


Figure 2. Comparative photodegradation evolution of At (a) and SMT (b) using different Ti-MOFs. For clarity, degradation of MOFs is omitted here (although included in the SI, Figure S2&S3).

MOF	Photodegraded At (%) MOF (%)	Kinetic constant ($M^{-1}\cdot h^{-1}$) R^2	Photodegraded SMT (%) MOF (%)	Kinetic constant ($M^{-1}\cdot h^{-1}$)
MIL-100(Ti)	100 ± 0 3.8 ± 0.1	12,199 0.985	100 ± 0 3.2 ± 0.3	112,013 0.964
MIL-100(Fe)	65.0 ± 4.4 9.7 ± 1.5	247 0.957	66.4 ± 10.4 1.0 ± 0.1	24,937 0.996
MIL-125-NH ₂	66.0 ± 1.1 38.8 ± 1.2	122,555 0.985	69.5 ± 5.2 39.3 ± 0.4	70,213 0.958
MUV-10(Ca)	43.9 ± 14.7 41.0 ± 1.9	64,034 0.995	34.4 ± 5.6 36.1 ± 6.4	4946 0.896
IEF-11	56.0 ± 12.6 0.78 ± 0.01 ^a	1124 0.982	0.00 ± 0.01 0.35 ± 0.01 ^a	–

Table 1. Total At and SMT photodegradation (after 5 h, %), MOF degradation (%), and kinetic constant ($M^{-1}\cdot h^{-1}$) for all studied materials. ^aValue corresponding to 24 h.

For comparison, the At and SMT adsorption capacity of the studied Ti-MOFs was performed in absence of light. As in the photocatalytic studies, the adsorption of At and SMT strongly depends on the MOF, decreasing in the following order: (At) MIL-125-NH₂ > MIL-100(Ti) > MUV-10(Ca); and (SMT) MIL-125-NH₂ > MIL-100(Ti) ~ MUV-10(Ca) (Figs. S2–S4). Unlike its remarkable pharmaceuticals photodegradation capacity, MIL-100(Ti) can eliminate by adsorption only 13.5 ± 3.9% of At and 0 ± 3.9% of SMT after 5 h. Again, in a view of providing a comparison, the same experiment was performed using the Fe-based MIL-100(Fe) analogue, obtaining similar adsorption capacities for At (8.2 ± 5.5%) and SMT (14.2 ± 8.0%) than the MIL-100(Ti). The formation of interactions between the At and the MIL-100(Ti) is evidenced by Fourier transform infrared spectroscopy (FTIR) by comparing the spectra of free At to that of the empty and the At loaded material (At@MIL-100(Ti)). Specifically, there is a shift in the wavelengths of pure At (from 2964 and 2922 cm^{-1} to 2955 and 2925 cm^{-1} for At and At@MIL-100(Ti), respectively; see SI, Figure S5), characteristic of the $\nu(C-H)$ group of the C9 (near the ether group C9–O–benzene)⁴⁰. In contrast, the MIL-125-NH₂ was able to adsorb up to 66.6 ± 1.1% of At and 50.2 ± 3.4% of SMT after 5 h. However, the release of the previously adsorbed EOCs was evidenced after 1 h, probably related with the degradation of the framework during the drug adsorption process (SI, Figure S2&S3). This is supported by the significant leaching of the linker (*ca.* 18% in both SMT and At adsorption after 5 h), confirmed by the similar FTIR spectra of the drug-loaded MIL-125-NH₂ and the free linker H₂BDC-NH₂ (SI, Fig S6), and the amorphization of the MIL-125-NH₂ framework after the adsorption process (SI, Figs. S7&S8).

On the other hand, it is imperative to get fast degradation kinetics in order to achieve more efficient removal processes. The comparison of the At and SMT degradation kinetics has been performed through the fitting of the data to a second order kinetics according to Eq. (1) (see experimental section and SI, Figure S9). Although the data have also been fitted to a zero and first order kinetics, a better correlation was found using the second order. This is in agreement with previously reported photoactive MOFs and composites (*i.e.*, MIL-125-NH₂ and AgNC@MIL-125-NH₂ in the degradation of SMT or methylene blue)¹². The best degradation rate is obtained when using MIL-125-NH₂ in the At degradation, with a k value of 122,555 $M^{-1}\cdot h^{-1}$, which is *ca.* 2, 10 and 109-fold higher than MUV-10(Ca), MIL-100(Ti), and IEF-11, respectively. In the case of SMT, the best degradation rate is obtained for MIL-100(Ti), with a k value of 112,013 $M^{-1}\cdot h^{-1}$, which is *ca.* 2, 5, and 23-fold higher than MIL-125-NH₂, MIL-100(Fe), and MUV-10(Ca), respectively. Finally, when evaluating the kinetics of the photocatalytic process using MIL-100(Ti) and MIL-125-NH₂, the *particle size* and the *external surface* may also play important roles. It is generally accepted that smaller particles might favor the catalytic reactions. Tentatively, we can argue that the smaller MIL-125-NH₂ particles (*ca.* 240 nm with an estimated external surface of 225 $mg^2\cdot g^{-1}$

by t-plot method (p/p_0 from 0.3 to 0.6)) than MIL-100(Ti) ($> 1 \mu\text{m}$ with an external surface of $195 \text{ mg}^2\text{-g}^{-1}$) will favor the transport of EOCs and degradation products.

Aside from the EOCs elimination capacity, the chemical stability of the framework is a limiting parameter in water decontamination processes. The point is to avoid an extra contamination of water due to the leaching of the MOFs constituents (e.g., ligands, metals). Therefore, and in contrast with the vast majority of reports on this topic, we have here considered the possible release of the MOF's building blocks. The chemical stability of a coordination network mainly depends on the strength of the metal to linker bonds, which can be estimated according to the hard and soft acids and bases (HSAB) principle⁴¹, and the competition with reactive species found in the solution. Thus, the release of the constitutive ligand was monitored by HPLC and the crystalline structure was checked by XRPD. At this point, it should be noted that the degradation of the frameworks was not evaluated via the quantification of the released metallic species in solution as, under the working conditions (contaminated tap water, pH = 8.2) and according to the Pourbaix diagram⁴², the vast majority of the degraded metallic species would be precipitated (i.e., TiO_2), underestimating the MOF degradation. Through the linker release, MOFs degradation could be also overestimated, as it can be adsorbed in the porosity of the framework (e.g., poorly activated/purified solids). However, we should rule out the release of any species that could be toxic, which is imperative for water decontamination. During the At and SMT photodegradation, the chemical stability of the framework in At or SMT-contaminated tap water decreased in the following order: (At) IEF-11 > MIL-100(Ti) > MIL-125-NH₂ ~ MUV-10(Ca); and (SMT) IEF-11 > MIL-100(Ti) > MUV-10(Ca) ~ MIL-125-NH₂ (Table 1). Note here that the stability ranking is very similar for At and SMT, ruling out an important effect of the drug nature on the MOF degradation. In addition, the XRPD patterns of the At- and SMT-containing MOFs evidenced that the At or SMT loading process does not alter the crystalline structure of MIL-100(Ti) and IEF-11, but there is an important peak broadening in the MUV-10(Ca) and MIL-125-NH₂ materials, consistent with a crystallinity loss (SI, Figure S7&S8). Remarkably, MIL-100(Ti) and IEF-11 show a high chemical stability under the working conditions with only ca. 3 and 0.7% degradation, respectively, after 5 h in contact with the contaminants' solutions.

Considering the above results, the most promising photocatalyst for the At and SMT removal in water is MIL-100(Ti), demonstrating not only an exceptionally high and fast EOCs degradation (100% in 2 and 4 h, respectively), but also a moderate matrix degradation (ca. 9%). This is particularly important considering that the median oral lethal dose (LD_{50}) for H₃BTC is ca. 4 times lower than the one for SMT and At (in rats, LD_{50} is 8.4, 2 and $> 2 \text{ g}\cdot\text{kg}^{-1}$ for H₃BTC, SMT and At). Therefore, the proposed photodegradation method is efficiently improving the water quality within a short time. The results on the photodegradation of At and SMT using MIL-100(Ti) are on the range or even overpass the results obtained with other MOFs, MOF composites or other materials (SI, Table S2).

At this point, in an attempt to rationalize the complex process involved in the At and SMT photodegradation using MIL-100(Ti), we have explored the photocatalytic performance of the isostructural iron analogue MIL-100(Fe) under equal conditions. It should be pointed that even the different band gap values of the Ti and Fe based MIL-100 materials (3.48 and 2.73 eV, respectively, SI, Figure S1), both suspensions were irradiated in all the UV-vis range. As expected, the Ti-based MIL-100 is more efficient than its Fe counterpart, with a 100% and ca. 65% of At and SMT degradation after 5 h-irradiation, evidencing the crucial role of the titanium trimeric clusters. When comparing the kinetic of the process (Table 1), the degradation rates of At and SMT by MIL-100(Ti) is ca. 49 and 4.5-fold higher than the Fe isostructural MOF. Both materials are chemically stable under the studied conditions, with only ca. 10 and 1% of MIL-100(Fe) degradation in At and SMT solutions, respectively. However, in the case of MIL-100(Fe), the degradation of the framework seems to be affected by the nature of the contaminant, being favored in the presence of At. The amide of At may preferentially interact with the Fe metal sites than with the Ti ones (more oxophilic). Finally, the accessible porosity of the framework is not a determining factor when comparing the Fe and Ti-based MIL-100 materials. Although the accessible porosity of MIL-100(Fe) is double than the one of MIL-100(Ti) (SI, Table S1), this last material is the most effective in At and SMT degradation.

Photodegradation products using MIL-100(Ti). The hazard of these EOCs does not only rely on their concentration or toxicity, but also their metabolites or degradation products, which can sometimes be more harmful than the parent compounds⁴³. The degradation products of At and SMT using MIL-100(Ti) were thus independently analyzed. Previous studies have described the photochemical behavior of At and SMT, determining that the degradation occurs through the cleavage at various positions (Figure S10)⁴⁴. The identification of the photodegradation products of At and SMT formed after 5 h-irradiation of the At@MIL-100(Ti) and SMT@MIL-100(Ti) systems in aqueous medium was carried out using UHPLC/MS, supported with fragmentation patterns obtained from MS/MS experiments. Although the determination of the EOCs degradation pathway is out of the scope of this work, we have successfully identified some intermediates deduced from their estimated molecular weight, allowing to assess the potential toxicity of the resulting products.

Particularly for At, cleavage of the side chain and the addition of the hydroxyl group to the parent compound were found to be the two main degradation pathways (Figures S10&S11). Thus, the fragment ion m/z 134 (3-(isopropyl)propane-1,2-diol) was attributed to the product from the chain cleavage, and the ions m/z 167 2-(2,4-dihydroxyphenyl)acetamide and 2-(3,4-dihydroxyphenyl)acetamide to the chain cleavage and oxidation. These photodegradation pathways and intermediates have been frequently reported in the photodegradation of At⁴⁵⁻⁴⁷.

On the other hand, in the SMT photodegradation study, the fragment ion m/z 216.7 (*N*-(4,6-dimethylpyrimidin-2-yl)benzene-1,4-diamine) was attributed to the product from SO₂ extrusion, a phenomenon frequently shown in sulfonamides (Figs. S10&S12)⁴⁸. The attack of a hydroxyl radical at the C-N bond of the benzene ring

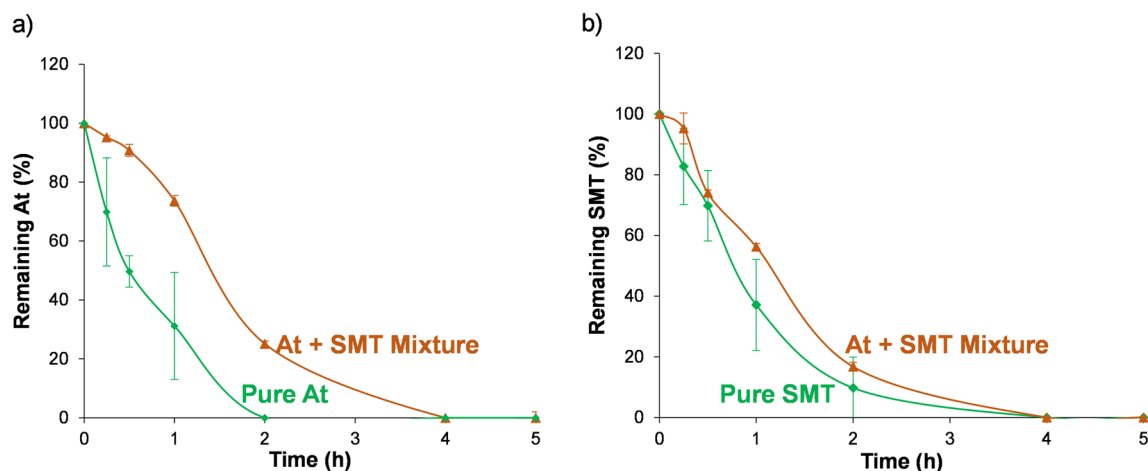


Figure 3. Effect of the mixture (brown, triangles) or single contaminants (green, diamonds) on the photodegradation of At (a) and SMT (b) using MIL-100(Ti).

EOCs	Photodegraded At (%)	Kinetic constant ($M^{-1}\cdot h^{-1}$) R^2	Photodegraded SMT (%)	Kinetic constant ($M^{-1}\cdot h^{-1}$)	MIL-100(Ti) degradation (%)
At	100 ± 0	12,199 0.985	–	–	3.8 ± 0.1
SMT	–	–	100 ± 0	112,013 0.964	3.3 ± 0.3
At + SMT	100 ± 0	2755 0.946	100 ± 0	45,835 0.966	1.34 ± 0.29

Table 2. Total combined At and SMT photodegradation (after 5 h, %), MOF degradation (%), and kinetic constant ($M^{-1}\cdot h^{-1}$) for MIL-100(Ti).

might result in the fragment derived from the pyrimidinyl portion (m/z 124), leading to the formation of the 2-amino-4,6-dimethoxypyrimidine product. The cracking of the N-containing benzene ring is attributed to the formation of the fragment ions m/z 197 (4-amino-N-(iminomethylene)benzenesulfonamide) and m/z 213 (4-(2-imino-4,6-dimethylpyrimidin-1(2H)-yl)cyclohexamine), as previously reported⁴⁹.

Importantly, regarding the potential toxicity of the degradation products, neither of the intermediated formed through At and SMT photodegradation exhibit acute toxicity⁴⁵, supporting then the significant improvement of the resulting water quality.

Combined EOCs photodegradation using MIL-100(Ti). In real water environments, physicochemical conditions are not static (e.g., presence of more than one pollutant with a different range of concentrations, or the pH of natural waters are normally found between 5 and 8)^{50,51}. Therefore, the target of an efficient photocatalyst should be the elimination of most of the EOCs present in this water in a range of different conditions (contaminants and catalyst concentration and contaminated water pH). In this context, first the At and SMT removal by MIL-100(Ti) was simultaneously investigated using a mixture of both contaminants in tap water (initial pH = 8.2). In this sense and to the best of our knowledge, there are no reported examples of the combined photodegradation of water EOCs using MOFs, but only the evaluation of their combined adsorption⁵². Remarkably, when both pollutants are present in solution, the time required to fully degrade the SMT is similar to the single SMT removal (100% of the SMT is removed in only 4 h, Fig. 3). In contrast, the At elimination is slowed down, and the time required to remove 100% of the At is doubled (from 2 to 4 h). The kinetics of the process is modified in both reactions, being the degradation rate reduced up to 4.5 and 2.4-fold for At and SMT, respectively (Table 2). This could be explained by the competitive degradation of SMT and At, where the SMT is favored over the At photodegradation. Regarding the MOF stability, in presence of both EOCs, the leaching of the H₃BTC linker is maintained, indicating the potential of the MIL-100(Ti) in the photodegradation of EOCs in water. In a further step to real conditions, other factors such as initial concentration of At and SMT, catalyst amount, and pH, were analyzed. The effect of the *initial concentration of contaminants* was studied using different At and SMT initial concentrations (from $C_0 = 35$ and 5 ppm to 17.5 and 2.5 ppm, respectively). MIL-100(Ti) degraded most of the SMT (95%) at low initial concentration, while the degradation efficiency of At decreased from 100% ($C_0 = 35$ ppm) to 15% ($C_0 = 17.5$ ppm) after 5 h irradiation. This phenomenon suggests that MIL-100(Ti) efficiently increases with EOCs concentration, which has great significance in more dangerous (toxic) environments. In agreement, no changes in the crystallinity or MIL-100(Ti) particles morphology are observed (SI, Figure S12).

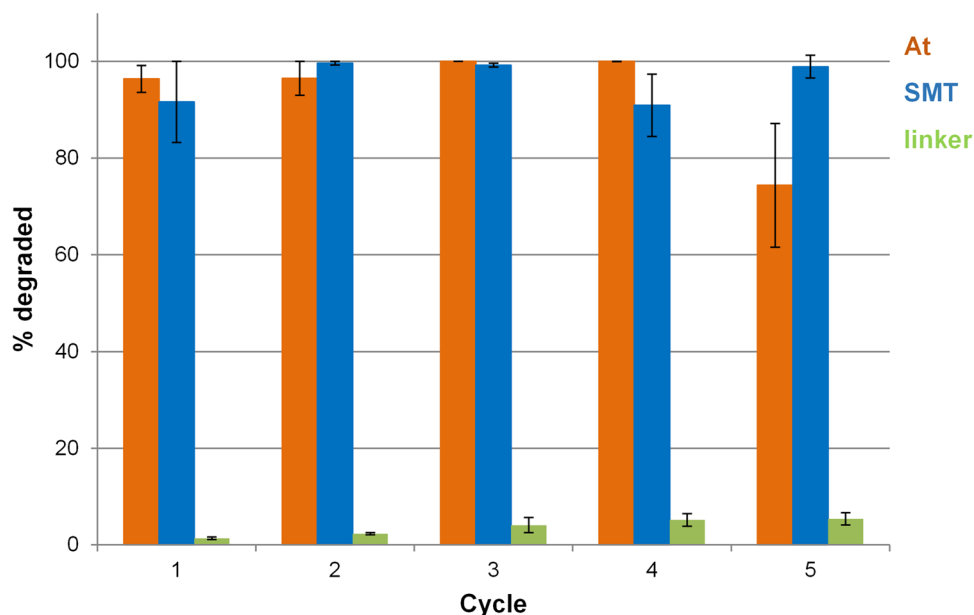


Figure 4. Cyclability tests of mixtures of SMT and At photodegradation in tap water using MIL-100(Ti).

On the other hand, when the *amount of catalyst* is reduced by half (from 4 to 2 mg), a high SMT removal (*ca.* 83%) is achieved, while the At removal capacity is considerably reduced (only *ca.* 44% in 5 h). In terms of MOF stability, the XRPD patterns showed that changes in contaminants concentration do not affect the crystallinity of MIL-100(Ti), while an important amorphization is observed when less amount of MIL-100(Ti) is used (SI, Figure S12). These results are supported by FESEM images, with important morphological changes in MIL-100(Ti) when the amount of MOFs is halved.

Finally, the *effect of pH* in At and SMT degradation was studied, by changing from an initial pH of contaminated water from 8.2 to 6.4 and 5.5. Under acidic conditions (pH = 6.5 and 5.5), the SMT elimination levels are maintained (*ca.* 90 and 91% of SMT degradation, respectively), while the At degradation capacity is strongly affected (only 27 and 9% of At is degraded in 5 h, respectively). Considering the pK_a of SMT ($pK_{a1} = 2.65$ -aromatic amine; $pK_{a2} = 7.65$ -sulfonamide) and the pK_a of At (9.6-amine), SMT is predominantly neutral (pH = 6.4 and 5.5) or protonated (pH = 8.2), while At is always protonated (pH = 5.5–8.2). Therefore, the protonation or deprotonation of the EOCs will not strongly affect the intermolecular electrostatic attraction between EOCs and MIL-100(Ti). However, considering that one of the interactions of the At with the MOF is through the central O of the At (according to FTIR, see above), it could be hypothesized that, as the attraction between the drug and the framework is stronger when the initial pH is higher, leading into a higher photocatalytic performance. The XRPD patterns demonstrated an amorphization under acidic conditions (SI, Figure S13). From the practical point of view, and although an optimization of the process is needed, we can conclude that the optimal working conditions for MIL-100(Ti) in SMT and At degradation are high EOCs concentrations (35 and 5 ppm, respectively), 4 mg of catalyst and alkaline waters.

Cyclability of MIL-100(Ti). The efficiency of a catalyst is significantly enhanced if the material can be re-used for several photodegradation cycles. After 5 h-irradiation, MIL-100(Ti) was recovered from the treated water by centrifugation, and resuspended in fresh contaminated water (mixture of contaminants). Upon 5 photodegradation cycles, MIL-100(Ti) efficiently removed SMT and At without a significant decrease on the efficiency (Fig. 4). Note here however that, upon the first and second cycles, an important peak broadening, consistent with a partial amorphization, is observed in the XRPD patterns (SI, Figure S14), leading to a completely amorphous solid after the third cycle. In contrast, the chemical integrity of MIL-100(Ti) is kept after the 5 cycles, with only 5% of the linker released. One could suggest that upon photocatalytic cycles, the chemical composition of the MIL-100(Ti) is almost kept, while the creation of defects leads to the loss of the long-range order, while improving the quality of water.

Conclusions

The screening of 4 robust Ti-MOFs for the removal of EOCs in tap water has allowed the selection of an extremely efficient photocatalyst, the mesoporous titanium trimesate MIL-100(Ti). Here, we present the successful photodegradation of the challenging EOCs, SMT and At, by this material, able to efficiently eliminate SMT and At (100% removal at 2 and 4 h, respectively) from tap water without an important chemical degradation. In addition, the generation of lower potential toxic products upon photodegradation supports the significant improvement of the quality of water. Further, when working with a contaminants mixture, the ability of MIL-100(Ti) to remove SMT is kept intact, while the At photodegradation is slowed-down, as a consequence of the drug competition. Upon 5 photodegradation cycles, MIL-100(Ti) efficiently removes both SMT and At, envisioning the future real

application of this MOF on the removal of SMT and At as well as other widespread EOCs in environmental remediation.

Methods

All reactants were commercially obtained and used without further purification. The synthesis of starting materials was performed following similar synthetic procedures as previously reported (see below).

Synthesis of MOFs. *Synthesis of MIL-100(Ti) or $[Ti_3(\mu_3-O)O(OH)_2(BTC)_2]^{33}$.* Ti_6 (7.2 mg, 24 μ mol of Ti) and trimesic acid (H_3BTC , 25.0 mg, 120 μ mol) were dispersed in 3 mL of a mixture of acetonitrile:tetrahydrofuran (ACN:THF, 3:1, v/v%) in a glass vial. Subsequently, 250 mL of acetic acid (180 equiv.) were added, and the mixture was sonicated to get a homogeneous suspension. The vial was placed in the oven at 160 °C for 48 h. After cooling down to room temperature (RT), the white microcrystalline powder was recovered by centrifugation at 5000 rpm for 2 min, rinsed with fresh *N,N*-dimethylformamide (DMF) and methanol (MeOH) and further purified by Soxhlet extraction with hot ethanol (EtOH) or MeOH for 8 h. The solid was then allowed to dry under vacuum at RT.

Synthesis of MIL-100 or $[Fe_3O(H_2O)_2OH(BTC)_2]^{53}$. $FeCl_3 \cdot 6H_2O$ (2.7 g, 10 mmol) and ethyl ester 1,3,5-benzenetricarboxylic (2.24 g, 6.66 mmol) were dispersed in 50 mL of deionized H_2O . The mixture was placed in a Teflon-lined autoclave at 130 °C for 3 days. Then, the orange solid was recovered by filtration and washed with absolute EtOH (3×10 mL). The solid was then suspended in 1 L of EtOH, refluxed under stirring for 3 h and then, the same procedure was performed in deionized water. Further activation was carried out by redispersing the solid in 100 mL of KF aqueous solution (0.1 M). The mixture was kept under magnetic stirring for 2 h and 40 min under ambient conditions. Immediately after, the solid was washed with water at room temperature by suspending the solid in 250 mL of water for 4 h. The solid was recovered by filtration.

Synthesis MUV-10(Ca) or $[Ti_3Ca_3(\mu_3-O)_3(BTC)_4]^{35}$. H_3BTC (125 mg, 595 μ mol) and $CaCl_2 \cdot 6H_2O$ (26.8 mg, 120 μ mol) were dissolved in a mixture of 12 mL of dry DMF and 3.5 mL of acetic acid in a 25 mL Schott bottle. Subsequently, titanium(IV) isopropoxide (36 μ L, 120 μ mol) was added to the clear solution. The bottle was sealed and heated in an oven at 120 °C for 48 h. After cooling down to RT, the microcrystalline powder was recovered by centrifugation at 5000 rpm for 2 min and rinsed with fresh DMF, water and MeOH several times and further purified by Soxhlet extraction with hot EtOH or MeOH for 8 h. The solid was then allowed to dry under vacuum at RT.

Synthesis of MIL-125-NH₂ or $[Ti_8O_8(OH)_4(BDC-NH_2)_6]^{34}$. 2-Aminoterephthalic acid ($H_2BDC-NH_2$, 1.38 g, 7.6 mmol) was dissolved in 20 mL of DMF and 5 mL of MeOH at RT under stirring. The mixture was placed in a round bottom flask (50 mL) equipped with a condenser and was warmed at 100 °C under air. When the mixture reached the temperature of 100 °C, 1.5 mL of titanium(IV) isopropoxide (1.5 g, 5.1 mmol) was added. The mixture was kept under magnetic stirring and heated for 72 h at 100 °C under air. The yellow solid obtained was filtered and washed with DMF at RT.

The as-synthesized dried product was dispersed at RT in DMF under stirring overnight (on, 100 mL of DMF per g of product). Then, the same procedure was repeated once using MeOH instead of DMF for 4 h.

Synthesis of IEF-11 or $[Ti_2O_3(SQ)]^{36}$. Finely ground squaric acid (H_2SQ , 255 mg, 2.24 mmol) was suspended in 8.2 mL of isopropanol in a 25 mL round-bottom flask, magnetically stirred for 5 min at RT and sonicated in an ultrasound bath for another 5 min. Then, glacial acetic acid (6.4 mL, 111.9 mmol) was added and sonicated again for 15 min. Then, titanium(IV) butoxide (762 μ L, 2.24 mmol) was slowly added to the previous solution under stirring and then, heated at 50 °C for 15 min. The resulting orange suspension was transferred into a 23 mL Teflon-lined steel autoclave, sealed and heated at 120 °C for 48 h with heating and cooling ramp of 1.5 °C·min⁻¹. The resulting orange-brown solid was filtered under vacuum, washed with isopropanol and dried in open air at RT. Finally, the sample was heated at 200 °C for 24 h in order to remove the remaining acetate moieties from the surface of the solid.

Experimental techniques. Fourier transform infrared spectroscopy (FTIR) studies were recorded using a Nicolet 6700 FTIR thermo scientific spectrometer in the 400–4000 cm⁻¹ region. X-ray powder diffraction (XRPD) patterns of all samples were collected in an Empyrean PANALYTICAL diffractometer, equipped with a PIXcel3D detector and a copper radiation source (Cu K α , $\lambda = 1.5406$ Å), operating at 45 kV and 40 mA. Profiles were generally collected in the $3^\circ < 2\theta < 35^\circ$ range with a typical step size of 0.013° and 40 s of acquisition.

N_2 isotherms were obtained at 77 K using a TriStar II Plus Instruments. Before the measurement, samples were evacuated under vacuum at 150 °C 16 h for MIL-100(Ti) and MUV-10(Ca), 200 °C 16 h for MIL-125-NH₂, and 130 °C 3 h for MIL-100(Fe). Specific surface area was determined by applying Brunauer, Emmett & Teller equation (BET) in the relative pressure interval $p/p_0 = 0.01-0.3$ (being p_0 the saturation pressure). External surface area was calculated by t-plot method in the relative pressure interval $p/p_0 = 0.3-0.6$. FESEM (Field Emission Scanning Microscope) JEOL JSM-7900F was used to obtain high resolution images of nanomaterials with magnifications from 20 to 1,000,000x and secondary electrons detector.

Different organic molecules were analyzed by HPLC: the amount of degraded sulfamethazine (SMT) and atenolol (At), as well as the released corresponding linkers ($H_2BDC-NH_2$ or H_3BTC), was determined using a reversed phase HPLC Jasco LC-4000 series system, equipped with a photodiode array (PDA) detector MD-4015

and a multisampler AS-4150 controlled by ChromNav software (Jasco Inc, Japan). A Purple ODS reverse-phase column (5 μm , 4.6×150 mm, Análisis Vínicos, Spain) was employed. For the quantification of all chemical species, isocratic conditions were used. The flow rate was $1 \text{ mL}\cdot\text{min}^{-1}$, and the column temperature was fixed at 298 K. In all cases, the injection volume was 30 μL . The mobile phase was based on a mixture of 50:50 MeOH:phosphate buffered solution (PBS, 0.04 M, pH = 2.5) for $\text{H}_2\text{BDC-NH}_2$ and H_3BTC ligands analysis, with a retention time (rt) and an absorption maximum of 2.84 min and 228 nm, and 3.51 min and 225 nm, respectively. SMT was analyzed using a mixture of 35:65 ACN:water, with a rt of 2.7 min and an absorption maximum of 263 nm. At was analyzed using a mixture of 10:90 ACN:PBS (0.04 M; pH = 2.5), rt = 4.81 min and $\lambda = 227$ nm.

Preparation of the PBS (0.04 M, pH = 2.5): 0.02 mol (2.4 g) of NaH_2PO_4 and 0.02 mol (2.84 g) of Na_2HPO_4 were dissolved in 1 L of Milli-Q water. The pH was then adjusted to 2.5 with H_3PO_4 .

Adsorption and/or photocatalytic degradation of SMT and/or At from water. The adsorption/photocatalytic activity of Ti-MOFs was evaluated in terms of elimination of both EOCs, SMT and At. In a typical experiment, 4 mg of MOF (MIL-100(Ti or Fe), MUV-10(Ca), MIL-125-NH₂ or IEF-11) were suspended in 4 mL of a SMT or At tap-aqueous solution (5 ppm⁵⁴, and 35 ppm^{22,23}, respectively; according with the concentration of SMT and At found in the environment). Adsorption/photodegradation reactions were performed under magnetic stirring. At certain intervals (0.25, 0.5, 1, 2, 4, and 5 h), an aliquot of 100 μL was collected by centrifugation for HPLC analysis (SMT, At and the corresponding ligand). All experiments were performed at least in triplicate to ensure statistically reliable results. The crystallinity of the remaining solids was analyzed by XRPD. First of all, the stability of an aqueous solution of SMT and At was studied under UV-vis light in absence of the photocatalyst. It was verified that SMT and At were not degraded (after 5 h) under UV-vis light irradiation.

SMT and At photodegradation products: Particularly in the At and SMT photodegradation studies, after 5 h of UV-vis irradiation, an aliquot was analyzed by mass quadrupole spectrometry coupled to ultra-high performance liquid chromatography (UHPLC) to determine the final products of the photodegradation. Standard samples of SMT and At were measured to deduce through comparison the mass parents obtained.

The photodegradation experiments were performed in a glass photoreactor equipped with a 300 W Xe lamp (Oriol Instrument OPSA500) under open air at RT, with the samples stirred and placed at a fixed distance of 21 cm from the irradiation source. It must be pointed that prior to irradiation it is not necessary to stir the suspension until the adsorption-desorption equilibrium is reached.

Although the selected Ti-based MOFs show a different experimental band gap (3.48, 2.73, 3.63, 2.53, and 2.40 eV for MIL-100(Ti), MIL-100(Fe), MUV-10(Ca), MIL-125-NH₂, and IEF-11, respectively; values obtained by the Tauc Plot, Supporting information-SI Figure S1)⁵⁵, we have irradiated all samples under the full UV-vis spectra. It should be noted that the use of a glass photoreactor may minimize the UV irradiation.

Combined At and SMT adsorption and/or photodegradation capacity of MIL-100(Ti): In an attempt to reproduce real water conditions, the same procedure was performed in a mixture of At and SMT in tap water. 4 mg of MIL-100(Ti) were suspended in 4 mL of a mixture of SMT (5 ppm) and At (35 ppm) tap-aqueous solution. Adsorption/photodegradation reactions were performed under stirring. At certain intervals (0.25, 0.5, 1, 2, 4, and 5 h), an aliquot of 100 μL was collected by centrifugation for HPLC analysis (SMT, At and H_3BTC ligand). If necessary, pH was adjusted with diluted solutions NaOH and HCl. All experiments were performed at least in triplicate to ensure statistically reliable results. The crystallinity of all the remaining solids was analyzed by XRPD.

Photodegradation kinetics: To shed some light on the At and SMT degradation kinetics and to gain further understanding on the involved mechanism, the first 2 h of At and SMT degradation were fitted to a second order kinetics according to Eq. (1),

$$\frac{1}{[A]} = \frac{1}{[A]_0} + kt \quad (1)$$

where $[A]$ and $[A]_0$ is the remaining concentration of contaminant (M, $\text{mol}\cdot\text{L}^{-1}$) at the time t (h) and the initial contaminant concentration, respectively, and k is the second order kinetic constant ($\text{M}^{-1}\cdot\text{h}^{-1}$).

Recyclability of MIL-100(Ti): The recyclability of MIL-100(Ti) was studied repeating the same procedure above described. 4 mg of MIL-100(Ti) were suspended in 4 mL of a mixture of At (35 ppm) and SMT (5 ppm) tap-aqueous solution under UV-vis light irradiation (considering the solubility of H_3BTC ($26.3 \text{ mg}\cdot\text{mL}^{-1}$), always working under sink conditions). After 5 h, the sample was centrifuged, an aliquot of 100 μL was collected for HPLC analysis (At, SMT and H_3BTC quantification), and the solid was resuspended again in a fresh At and SMT aqueous solution for 24 h. This process was repeated for 5 cycles.

Data availability

The datasets used and/or analysed during the current study available from the corresponding author on request.

Received: 6 May 2022; Accepted: 16 August 2022

Published online: 25 August 2022

References

1. Heberer, T. Tracking persistent pharmaceutical residues from municipal sewage to drinking water. *J. Hydrol.* **266**, 175–189 (2002).
2. Touraud, E., Roig, B., Sumpter, J. P. & Coetsier, C. Drug residues and endocrine disruptors in drinking water: Risk for humans?. *Int. J. Hyg. Environ. Health* **214**, 437–441 (2011).
3. Jurado, A. *et al.* Emerging organic contaminants in groundwater in Spain: A review of sources, recent occurrence and fate in a European context. *Sci. Total Environ.* **440**, 82–94 (2012).
4. Sharma, V. K. & Feng, M. Water depollution using metal-organic frameworks-catalyzed advanced oxidation processes: A review. *J. Hazard. Mater.* **372**, 3–16 (2019).

5. Fei, J. *et al.* Recent advances in graphitic carbon nitride as a catalyst for heterogeneous Fenton-like reactions. *Dalt. Trans.* **50**, 16887–16908 (2021).
6. Li, H., Eddaoudi, M., O’Keeffe, M. & Yaghi, O. M. Design and synthesis of an exceptionally stable and highly porous metal-organic frameworks. *Nature* **402**, 276–279 (1999).
7. Alvaro, M., Carbonell, E., Ferrer, B., Llabrés I Xamena, F. X. & Garcia, H. Semiconductor behavior of a metal-organic framework (MOF). *Chem.–A Eur. J.* **13**, 5106–5112 (2007).
8. Zhu, J., Li, P. Z., Guo, W., Zhao, Y. & Zou, R. Titanium-based metal–organic frameworks for photocatalytic applications. *Coord. Chem. Rev.* **359**, 80–101 (2018).
9. Chen, X. *et al.* Recent advances in titanium metal–organic frameworks and their derived materials: Features, fabrication, and photocatalytic applications. *Chem. Eng. J.* **395**, 125080 (2020).
10. Nguyen, H. L. The chemistry of titanium-based metal-organic frameworks. *New J. Chem.* **41**, 14030–14043 (2017).
11. Wang, H. *et al.* Controllable self-assembly of CdS@NH₂-MIL-125(Ti) heterostructure with enhanced photodegradation efficiency for organic pollutants through synergistic effect. *Mater. Sci. Semicond. Process.* **97**, 91–100 (2019).
12. Arenas-Vivo, A. *et al.* Ultrafast reproducible synthesis of an Agnanocluster@MOF composite and its superior visible-photocatalytic activity in batch and in continuous flow. *J. Mater. Chem. A* **9**, 15704–15713 (2021).
13. Patel, M. *et al.* Pharmaceuticals of emerging concern in aquatic systems: Chemistry, occurrence, effects, and removal methods. *Chem. Rev.* **119**, 3510–3673 (2019).
14. Spanish National Health System. *Sanidad en datos*. <https://www.mscbs.gob.es/estadEstudios/sanidadDatos/home.htm> (2021).
15. Spanish Agency for Medicines and Health Products. (2021).
16. The Spanish Agency of Medicines and Medical Devices. *Commonly consumed antihypertensive drugs with official prescription*. <https://www.aemps.gob.es/medicamentos-de-uso-humano/observatorio-de-uso-de-medicamentos/informes/> (2021).
17. Allothman, Z. A., Badjah, A. Y., Alharbi, O. M. L. & Ali, I. Cobalt doping of titanium oxide nanoparticles for atenolol photodegradation in water. *Environ. Sci. Pollut. Res.* **28**, 7423–7430 (2021).
18. Jones, R. G., Groeger, L. V. & Ornstein, C. *Prescriber Checkup*. <https://projects.propublica.org/checkup/> (2019).
19. Rastogi, T., Leder, C. & Kümmerer, K. A sustainable chemistry solution to the presence of pharmaceuticals and chemicals in the aquatic environment—the example of re-designing β -blocker Atenolol. *RSC Adv.* **5**, 27–32 (2015).
20. Haro, N. K., Del Vecchio, P., Marcilio, N. R. & Féris, L. A. Removal of atenolol by adsorption e study of kinetics and equilibrium. *J. Clean. Prod.* **154**, 214–219 (2017).
21. H. Jones, O. A., Voulvoulis, N. & Lester, J. N. Human Pharmaceuticals in Wastewater Treatment Processes. *Crit. Rev. Environ. Sci. Technol.* **35**, 401–427 (2005).
22. Vieno, N., Tuhkanen, T. & Kronberg, L. Elimination of pharmaceuticals in sewage treatment plants in Finland. *Water Res.* **41**, 1001–1012 (2007).
23. Lee, H., Sarafin, K. & Peart, T. E. Determination of B-blockers and B₂-agonists in sewage by solid-phase extraction and liquid chromatography–tandem mass spectrometry. *J. Chromatogr. A* **1148**, 158–167 (2007).
24. Anadón, A., Martínez-Larrañaga, M. R., Ares, I., Castellano, V. & Martínez, M. A. Drugs and chemical contaminants in human breast milk. In: *Reproductive and Developmental Toxicology* 68–95 (2017). doi:<https://doi.org/10.1016/b978-0-12-804239-7.00005-6>.
25. Carvalho, I. T. & Santos, L. Antibiotics in the aquatic environments: A review of the European scenario. *Environ. Int.* **94**, 736–757 (2016).
26. *Consumption maps. National Plan of Resistant Antibiotics* (2021).
27. European Medicines Agency & Agency. *Sales of veterinary antimicrobial agents in 31 European countries in 2017 (EMA/294674/2019)*. https://www.ema.europa.eu/en/documents/report/sales-veterinary-antimicrobial-agents-31-european-countries-2017_en.pdf (2019).
28. Vila-Costa, M. *et al.* Degradation of sulfonamides as a microbial resistance mechanism. *Water Res.* **115**, 309–317 (2017).
29. Hruska, K. & Franek, M. Sulfonamides in the environment: A review and a case report. *Vet. Med. (Praha)* **57**, 1–35 (2012).
30. Bialk-Bielińska, A. *et al.* Ecotoxicity evaluation of selected sulfonamides. *Chemosphere* **85**, 928–933 (2011).
31. Zhang, K. *et al.* Antibiotic resistance genes in drinking water of China: Occurrence, distribution and influencing factors. *Ecotoxicol. Environ. Saf.* **188**, 109837 (2020).
32. DeSantis, D. *et al.* Techno-economic analysis of metal-organic frameworks for hydrogen and natural gas storage. *Energy Fuels* **31**, 2024–2032 (2017).
33. Castells-Gil, J. *et al.* De novo synthesis of mesoporous photoactive titanium(IV)-organic frameworks with MIL-100 topology. *Chem. Sci.* **10**, 4313–4321 (2019).
34. Dan-Hardi, M. *et al.* A new photoactive highly porous titanium (IV) dicarboxylate. *J. Am. Chem. Soc.* **131**, 10857–10859 (2009).
35. Castells-Gil, J. *et al.* Chemical engineering of photoactivity in heterometallic titanium-organic frameworks by metal doping. *Angew. Chemie-Int. Ed.* **57**, 8453–8457 (2018).
36. Salcedo-Abraira, P. *et al.* A novel porous Ti-squarate as efficient photocatalyst in the overall water splitting reaction under simulated sunlight irradiation. *Adv. Mater.* **33**, 2106627 (2021).
37. Quadra, G. R. *et al.* Temporal and spatial variability of micropollutants in a Brazilian urban river. *Arch. Environ. Contam. Toxicol.* **81**, 142–154 (2021).
38. Chow, L. K. M., Ghaly, T. M. & Gillings, M. R. A survey of sub-inhibitory concentrations of antibiotics in the environment. *J. Environ. Sci. (China)* **99**, 21–27 (2021).
39. Fekadu, S., Alemayehu, E., Dewil, R. & Van der Bruggen, B. Pharmaceuticals in freshwater aquatic environments: A comparison of the African and European challenge. *Sci. Total Environ.* **654**, 324–337 (2019).
40. de Castro, R. A. E., Canotilho, J., Barbosa, R. M. & Redinha, J. S. Infrared spectroscopy of racemic and enantiomeric forms of atenolol. *Spectrochim. Acta-Part A Mol. Biomol. Spectrosc.* **67**, 1194–1200 (2007).
41. Pearson, R. G. Hard and soft acids and bases. *J. Am. Chem. Soc.* **85**, 3533–3539 (1963).
42. Pourbaix, M. *Atlas of Electrochemical Equilibria in Aqueous Solutions*. National Association of Corrosion Engineers: Englewood. (1974).
43. Brienza, M. *et al.* Use of solar advanced oxidation processes for wastewater treatment: Follow-up on degradation products, acute toxicity, genotoxicity and estrogenicity. *Chemosphere* **148**, 473–480 (2016).
44. Jia, M. *et al.* Integrating N and F co-doped TiO₂ nanotubes with ZIF-8 as photoelectrode for enhanced photo-electrocatalytic degradation of sulfamethazine. *Chem. Eng. J.* **388**, 124388 (2020).
45. Medana, C. *et al.* Characterization of atenolol transformation products on light-activated TiO₂ surface by high-performance liquid chromatography/high-resolution mass spectrometry. *Rapid Commun. mass Spectrom.* **22**, 301–313 (2008).
46. Yang, H., Li, G., An, T., Gao, Y. & Fu, J. Photocatalytic degradation kinetics and mechanism of environmental pharmaceuticals in aqueous suspension of TiO₂: A case of sulfa drugs. *J. Hazard. Mater.* **179**, 834–839 (2010).
47. Ji, Y. *et al.* Photocatalytic degradation of atenolol in aqueous titanium dioxide suspensions: Kinetics, intermediates and degradation pathways. *J. Photochem. Photobiol. A Chem.* **254**, 35–44 (2013).
48. Ji, Y. *et al.* Sulfate radical-based oxidation of antibiotics sulfamethazine, sulfapyridine, sulfadiazine, sulfadimethoxine, and sulfa-chloropyridazine: Formation of SO₂ extrusion products and effects of natural organic matter. *Sci. Total Environ.* **593–594**, 704–712 (2017).

49. Wang, N. *et al.* Photocatalytic degradation of sulfonamides by Bi₂O₃-TiO₂/PAC ternary composite: Mechanism, degradation pathway. *J. Water Process Eng.* **36**, 101335 (2020).
50. Federal-Provincial-Territorial Committee on Drinking Water. *Guidelines for Canadian Drinking Water Quality*. <https://www.canada.ca/content/dam/hc-sc/documents/services/publications/healthy-living/guidelines-canadian-drinking-water-quality-guide-line-technical-document-ph-eng.pdf> (2015) doi:978-0-660-04436-1.
51. EPA. United States Environmental Protection Agency. *CADDIS Volume 2* <https://www.epa.gov/caddis-vol2/ph> (2022).
52. Chen, C. *et al.* Adsorption behaviors of organic micropollutants on zirconium metal-organic framework UiO-66: Analysis of surface interactions. *ACS Appl. Mater. Interfaces* **9**, 41043–41054 (2017).
53. Horcajada, P. *et al.* Synthesis and catalytic properties of MIL-100(Fe), an iron(III) carboxylate with large pores. *Chem. Commun.* **100**, 2820–2822 (2007).
54. Petrovic, M. & Verlicchi, P. Water treatment plants and pharmaceutical residues in Catalonia and Italy. *Contrib. to Sci.* **10**, 135–150 (2014).
55. Viezicke, B. D., Patel, S., Davis, B. E. & Birnie, D. P. Evaluation of the Tauc method for optical absorption edge determination: ZnO thin films as a model system. *Phys. status solidi* **252**, 1700–1710 (2015).

Acknowledgements

This research is part of the projects PID2019-104228RB-I00, PID2020-118117RB-I00, RTC2019-007254-5, and the Maria de Maeztu IMDEA Energy Institute founded by MCIN/AEI/10.13039/501100011033. SR wants to acknowledge Regional Madrid funding (Talento 2017 Modality 2, 2017-T2/IND-5149), and Juan de la Cierva incorporation grant JC2019-038894-I founded by MCIN/AEI/10.13039/501100011033. SR and PH acknowledge grant RED2018-102471-T founded by MCIN/AEI/10.13039/501100011033. NMP thanks the Generalitat Valenciana (SEJIGENT/2021/059 and PROMETEU/2021/054) and La Caixa Foundation for a Postdoctoral Junior Leader–Retaining Fellowship (ID 100010434 and fellowship code LCF/BQ/PR20/11770014).

Author contributions

All authors reviewed the manuscript.

Competing interests

The authors declare no competing interests.

Additional information

Supplementary Information The online version contains supplementary material available at <https://doi.org/10.1038/s41598-022-18590-1>.

Correspondence and requests for materials should be addressed to S.R. or P.H.

Reprints and permissions information is available at www.nature.com/reprints.

Publisher's note Springer Nature remains neutral with regard to jurisdictional claims in published maps and institutional affiliations.



Open Access This article is licensed under a Creative Commons Attribution 4.0 International License, which permits use, sharing, adaptation, distribution and reproduction in any medium or format, as long as you give appropriate credit to the original author(s) and the source, provide a link to the Creative Commons licence, and indicate if changes were made. The images or other third party material in this article are included in the article's Creative Commons licence, unless indicated otherwise in a credit line to the material. If material is not included in the article's Creative Commons licence and your intended use is not permitted by statutory regulation or exceeds the permitted use, you will need to obtain permission directly from the copyright holder. To view a copy of this licence, visit <http://creativecommons.org/licenses/by/4.0/>.

© The Author(s) 2022